# Fundamental High-Pressure Calibration from All-Electron Quantum Monte Carlo Calculations

K. P. Esler,[1,2,*] R. E. Cohen,[1] B. Militzer,[3] Jeongnim Kim,[2] R. J. Needs,[4] and M. D. Towler[4]

[1]*Geophysical Laboratory, Carnegie Institution of Washington, Washington, D.C. 20015, USA*

[2]*NCSA, University of Illinois at Urbana-Champaign, Urbana, Illinois 61801, USA*

[3]*Department of Earth and Planetary Science and of Astronomy, University of California Berkeley, Berkeley, California 94720, USA*

[4]*TCM Group, Cavendish Laboratory, Cambridge CB3 0HE, United Kingdom*

(Received 22 September 2009; revised manuscript received 15 October 2009; published 5 May 2010)

We develop an all-electron quantum Monte Carlo (QMC) method for solids that does not rely on pseudopotentials, and use it to construct a primary ultra-high-pressure calibration based on the equation of state of cubic boron nitride. We compute the static contribution to the free energy with the QMC method and obtain the phonon contribution from density functional theory, yielding a high-accuracy calibration up to 900 GPa usable directly in experiment. We compute the anharmonic Raman frequency shift with QMC simulations as a function of pressure and temperature, allowing optical pressure calibration. In contrast to present experimental approaches, small systematic errors in the theoretical EOS do not increase with pressure, and no extrapolation is needed. This all-electron method is applicable to first-row solids, providing a new reference for *ab initio* calculations of solids and benchmarks for pseudopotential accuracy.

DOI: 10.1103/PhysRevLett.104.185702 PACS numbers: 64.30.Jk, 02.70.Ss, 63.20.dk, 81.05.Je

Although the number of density-functional-theory (DFT) studies continues to grow explosively, the accuracy of their predictions is variable, limiting confidence in DFT results as a quantitative calibration for experimental studies. The quantum Monte Carlo (QMC) technique is the highest-accuracy method for finding the ground state of a many-electron Hamiltonian. For solids with atoms heavier than He, however, the Hamiltonian itself is approximated using pseudopotentials (PPs) based on a lower-accuracy theory, limiting its reliability, and as we show, commonly used PPs give disparate results. In this Letter, we push the state of the art in accuracy by introducing a method for an all-electron DMC simulation of solids, eliminating the bias from pseudopotentials, and apply it to create a high-accuracy pressure calibration scale.

The combination of ultra-high-pressure mineralogy with seismology has yielded a wealth of insight into the internal structure of our planet. Pressure is the key that links these disciplines, mapping phase transitions and mineral properties to planetary depth. Establishing an absolute pressure calibration at multimegabar pressures poses a fundamental and continuing problem for high-pressure experiments. Primary calibrations are based on data from shock-wave experiments, which infer pressure from conservation of momentum and energy as the shock traverses the sample. Scales differ from each other by as much as 7% at room temperature, with even greater discrepancies at high temperature [1]. Such disparity remains a serious obstacle to a quantitative understanding of Earth's interior.

A pressure calibrant is a material with a known equation of state (EOS), placed in hydrostatic equilibrium with the test subject (e.g., ruby [2]). High-pressure Brillouin scattering, in conjunction with x-ray diffraction measurements of volume, can be integrated to provide an EOS, but a correction must be made to transfer from an adiabatic to an isothermal path [3]. New approaches such as quasiadiabatic *Z*-pinch based experiments [4,5] also hold future promise for a primary scale. There have been attempts to refine the ruby scale [6], and new calibrations have been suggested [3]. Cubic boron nitride (*c*-BN) has been identified as a promising material for a new scale [7]. We provide a new pressure scale based on diffusion Monte Carlo (DMC) calculations of the EOS and Raman frequency of *c*-BN. This theoretical approach has the advantage that the method works equally well under high compression, and uncertainty does not grow with pressure.

In a wide-gap insulator such as *c*-BN, the free energy can be written as a sum of the frozen lattice enthalpy, dependent only on volume, and a phonon thermal free energy, which depends on both volume and temperature. Since the static enthalpy dominates contribution at ordinary temperatures, errors in a theoretical EOS can most often be attributed to the static part. Previous calculations of the EOS of *c*-BN have been based on DFT [7], which use approximate functionals to treat electron exchange and correlation. Several functionals are in common use, each giving rise to a different EOS, with no *a priori* way to predict which will give the most reliable result.

QMC methods explicitly treat electron exchange and correlation instead of resorting to approximate functionals. Diffusion Monte Carlo samples the many-body ground state of the Hamiltonian through a stochastic projection of the trial function. In practice, a fixed-node approximation is used for fermions, such as electrons, which gives relatively small errors when the nodes are obtained from high-quality DFT orbitals for electronically simple materials such as *c*-BN. DMC for solids has been demonstrated to give significantly more accurate cohesive energies [8], equations of state and Raman frequencies [9], and phase

 

TABLE I. Parameters for the $c$-BN EOS and Raman calibration.

(a) Parameters for 300 K EOS

| Source (# of atoms) | $V_0$ (Å$^3$) | $B_0$ (GPa) | $B_0'$ |
|---|---|---|---|
| TN PP(64)/AE(8) | 11.792(18) | 381(6) | 3.87(6) |
| WC PP(64)/AE(8) | 11.769(17) | 385(6) | 3.86(6) |
| BFD PP(64)/AE(8) | 11.781(20) | 382(7) | 3.87(7) |
| BFD PP(128)/AE(16) | 11.812(8) | 378(3) | 3.87(3) |
| Datchi *et al.*[24] | 11.8124 | 395(2) | 3.62(5) |
| Goncharov *et al.* | 11.817(32) | 387(4) | 3.06(15) |

(b) Parameters for thermal pressure

| $n$ | $\theta_n^0$(K Å$^{-3n}$) | $\alpha_n$(K$^{-1}$ Å$^{-3n}$) | $\beta_n$(K Å$^{-3n}$) |
|---|---|---|---|
| 0 | $4.836\,66 \times 10^{3}$ | $2.598\,61 \times 10^{-3}$ | $-4.869\,56 \times 10^{3}$ |
| 1 | $-6.929\,70 \times 10^{1}$ | $-1.200\,50 \times 10^{-4}$ | $1.763\,44 \times 10^{2}$ |
| 2 | $4.634\,28 \times 10^{-1}$ | $2.789\,13 \times 10^{-6}$ | $-2.186\,05 \times 10^{0}$ |
| 3 | $-1.273\,47 \times 10^{-3}$ | $-2.008\,99 \times 10^{-8}$ | $9.303\,18 \times 10^{-3}$ |

(c) Parameters for Raman calibration

| $n$ | $c_n$(cm$^{-1}$) | $R_n$ (GPa) | $b$ |
|---|---|---|---|
| 0 | 1055.9 | 349.87 | 3.0155 |
| 1 | −144.24 | 1849.4 | |
| 2 | 1497.8 | 112.33 | |

transitions [10] than DFT. We have used both the CASINO QMC software suite [11] and QMCPACK [12].

QMC simulations of solids are currently performed within the pseudopotential (PP) approximation, in which the core electrons are replaced by a nonlocal potential operator [8]. Since PPs are presently constructed with a lower-accuracy theory, such as Hartree-Fock (HF) or DFT, this replacement represents an uncontrolled approximation. To eliminate this error, we develop a method for all-electron (AE) QMC simulations of solids in QMCPACK using trial wave functions derived from full-potential linearized augmented plane wave (FP-LAPW) calculations using the EXCITING code [13]. Space is divided into spherical *muffin tin* regions around the nuclei, and an interstitial region. Orbitals are represented inside the muffin tins as a product of radial functions and spherical harmonics, and outside as plane-waves. To ensure that a wave function satisfies the variational principle, it must be both continuous and smooth. We utilize a *super*-LAPW formalism that enforces continuity and smoothness at the muffin tin boundary. For efficiency, we represent the orbitals as 3D $B$ splines in the interstices and the product of radial splines and spherical harmonics in the muffin tins.

Since AE QMC simulations are computationally expensive, we perform these simulations in 8-atom cubic supercells. Simulation cells this small would typically have significant finite-size errors. By combining data from AE and PP simulations performed in both 8- and 64-atom supercells, we simultaneously eliminate systematic errors from PPs and finite-size effects. The corrected static-lattice energy is given at each volume as

$$E = E_{64}^{\mathrm{PP}} + [E_8^{\mathrm{AE}} - E_8^{\mathrm{PP}}] + \Delta_{64}^{\mathrm{MPC}} + \Delta_{64}^{\mathrm{kinetic}}, \quad (1)$$

where the term in brackets removes the pseudopotential bias. $\Delta_{64}^{\mathrm{MPC}}$ and $\Delta_{64}^{\mathrm{kinetic}}$ are, respectively, potential [14] and kinetic [15] corrections for finite-size errors. We perform this procedure with three different PP sets commonly used in the QMC simulations: HF PPs from Trail and Needs (TN) [16]; HF PPs from Burkatzki, Filippi, and Dolg (BFD) [17]; and DFTGGA [18] PPs generated with OPIUM (WC) [19]. Performing the same procedure with 128-atom PP simulations and 16-atom AE simulations yields statistically indistinguishable results, demonstrating that finite-size errors are converged. Additional details are in the supplementary material [20].

To compute the phonon free energy, we use density functional perturbation theory (DFPT) in the QUANTUM ESPRESSO package [21] with the Wu-Cohen functional and the OPIUM PPs. The phonon density of states, from which we derive thermodynamic data, is usually very well-described with DFT.

We compute the free energy for our $c$-BN system at 12 unit-cell volumes, spanning volume compression ratios from 0.84 to 2.0, corresponding to pressures of about −50 GPa to 900 GPa. Theoretical studies have not identified any structural transition below 1 TPa [22], nor has one been observed experimentally. We use the Vinet form [23] for the isothermal EOS, which we find represents our free energy data very well, yielding the bulk modulus, $B_0$, its pressure derivative, $B_0'$, and the equilibrium volume, $V_0$ [Table I(a)]. From our QMC error bars, we compute statistical confidence ranges, taking into account parameter cross-correlations with a simple Monte Carlo procedure.

Figure 1 shows the EOS of $c$-BN at 300 K, with experimental data from Datchi *et al.* [24] and Goncharov *et al.* [7], as well as the present work from simulations with three different PPs. The residuals in (c) are derived from DMC simulation with PPs alone, while those in (b) combine all-electron and PP data. The discrepancy between the theoretical curves in (c), suggests that PP simulation alone does not provide sufficient accuracy. Once the PP data is combined with AE data, as in (b), all the theoretical curves come into good agreement. Our theoretical EOS agrees with that in Refs. [7,24] within the experimentally measured pressure range, but the experimental extrapolation shows significant deviation at high pressure.

We may write the thermal equation of state in the form

$$P(V,T) = P_{300\,\mathrm{K}}(V) + P_{\mathrm{th}}(V,T) - P_{\mathrm{th}}(V,T=300), \quad (2)$$

where $P_{300\ \mathrm{K}}$ is the room-temperature contribution, fitted to the Vinet form. The phonon contribution is fitted to an augmented Debye model,

$$P_{\mathrm{th}}(V,T) = -\frac{\partial F_D(\theta,T)}{\partial \theta}\frac{\partial \theta}{\partial V} \quad (3)$$

$$\theta(V,T) = \theta^0(V) + \beta(V)\exp(-\alpha(V)T) \quad (4)$$

$$x(V) = x_0 + x_1 V + x_2 V^2 + x_3 V^3, \quad x = \theta^0, \quad \alpha \text{ or } \beta \quad (5)$$

in which the Debye temperature, $\theta$, is a function of both $V$ and $T$ [Table I(b)]. The Debye free energy per two-atom cell, excluding the zero-point term, is given by

$$F_D = 6k_B T\left[\ln\left(1 - e^{\theta/T}\right) - \left(\frac{\theta}{T}\right)^3 \int_0^{\theta/T} \frac{x^3}{e^x - 1} dx\right]. \quad (6)$$

$c$-BN can be used to calibrate pressure optically by measuring the frequency shift of the TO Raman mode. We compute the pressure and temperature dependence of this frequency. Within the quasiharmonic approximation, phonon frequencies have explicit dependence on volume only. At constant pressure, however, an implicit $T$ dependence arises from thermal expansion. This accounts for only about half the total $T$ dependence of the Raman mode, as observed in [25,26]. The remaining dependence results from significant anharmonic effects in $c$-BN, which we include in our calculations.

Since the optical branch has small dispersion, we treat the anharmonicity as a 1D on-site anharmonic oscillator, in a similar approach to the QMC computation of the TO Raman frequency of diamond [9]. At each volume, we compute the effective Born-Oppenheimer potential well for the TO mode with DMC and the BFD PP at nine displacements along the mode eigenvector in the 64-atom supercell. We fit the data to a quartic polynomial, and numerically solve the 1D Schrödinger equation in this analytic potential. This results in a set of single-phonon energy levels, $\{E_n\}$, with nonuniform separation. From $\{E_n\}$, we compute an intensity-weighted average Raman frequency, $\bar{\nu}$, as a function of pressure and temperature. The matrix element for the transition from $n$ to $n-1$ is proportional to $\sqrt{n}$ and is weighted by the Boltzmann occupation of state $n$, so the intensity-averaged frequency, $\langle\nu\rangle$ is

$$\langle\nu\rangle = \frac{\sum_{n=1}^{\infty} I_n \frac{E_n - E_{n-1}}{hc}}{\sum_{n=1}^{\infty} I_n}, \quad \text{where } I_n = n e^{-(E_n)/k_B T}. \quad (7)$$

The excess thermal softening, i.e., beyond that from thermal expansion alone, is accounted for by the thermal average of the anharmonic frequencies. Figure 2 shows the computed Raman frequencies compared with the experimental data reported in Refs. [25–27].

Both Refs. [25,26] give a rubylike calibration formula, which can be expressed as

$$P = (R/b)[(\nu/\bar{\nu})^b - 1], \quad (8)$$

where $R$, $\bar{\nu}$, and $b$ have quadratic $T$ dependence. This dependence is sufficient below 2000 K, but cannot represent our data at high temperature. We use a form which captures the Boltzmann occupation of phonon excitations,

$$\nu(P, T) = \nu_0(P) + \nu_1(P) \exp\left[-\frac{\nu_2(P)}{T}\right], \quad (9)$$

$$\nu_n(P) = c_n\left[\frac{bP}{R_n} + 1\right]^{1/b}, \qquad n = 1, 2, 3 \quad (10)$$

with parameters in Table I(c) and plotted in Fig. 2(a). Note that this formula cannot be analytically inverted, but a very simple iterative solution can be used for calibrating pressure from $\nu$ and $T$.

The main axis of Fig. 2(b) gives the Raman frequency versus pressure at 300 K. There is good agreement in the relatively low-pressure region in which the Raman frequency was measured. At very high pressure, the deviation with respect to the extrapolation in [25] increases with a maximum discrepancy of 38 $\text{cm}^{-1}$ or, conversely, a deviation in the pressure calibration of 50 GPa at 900 GPa. The deviations with respect to [26] are 70 $\text{cm}^{-1}$ and 120 GPa. The experimental parameters capture the correct qualitative high-pressure behavior up to 900 GPa, despite the fact that data was available only to 20 and 64 GPa, respectively. This suggests the form for the fit was well chosen.

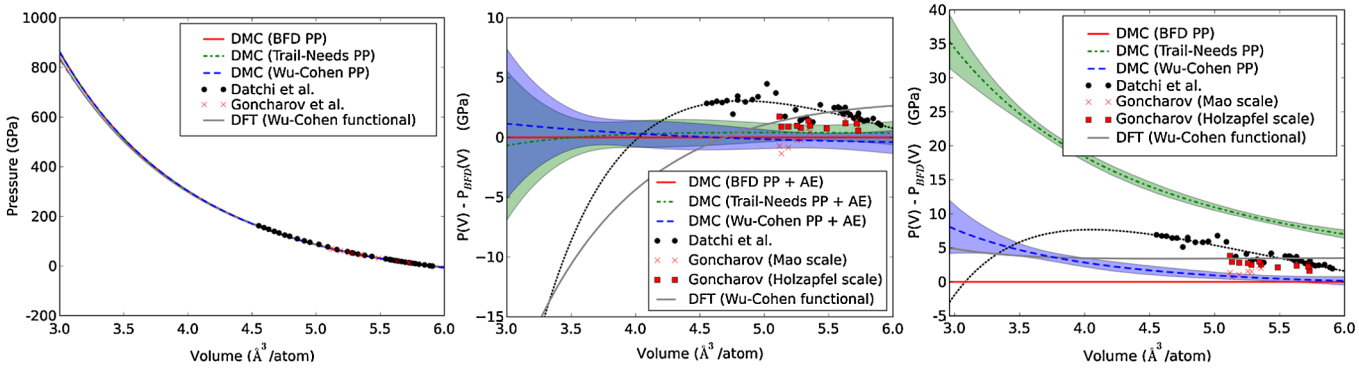


(a) Corrected EOS (b) Corrected pressure residuals (c) Uncorrected pressure residuals

FIG. 1 (color online). The $c$-BN EOS at 300 K, computed with DMC, compared to experiment. We plot the full EOS and the pressure residuals with respect to DMC with the BFD PP. (a) gives the corrected EOS resulting from combining the EOS and PP data, while (b) gives the pressure residuals for the same data. (c) gives the uncorrected pressure residuals from the PP simulations only. Shaded areas represent the one-$\sigma$ statistical confidence region from QMC data.

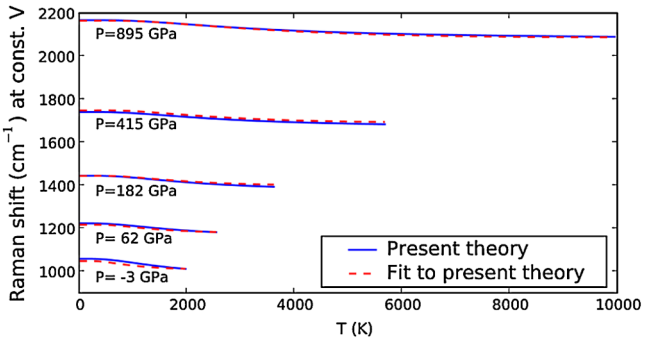


(a) Fit to present theory for Raman shift.

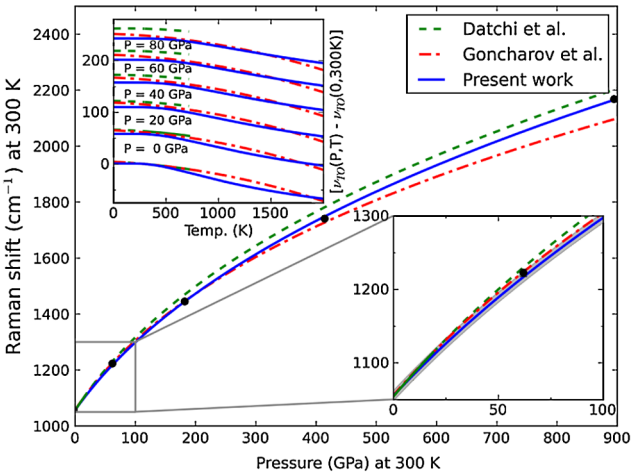


(b) Comparison of Raman experiment and theory.

FIG. 2 (color online). TO Raman frequency of $c$-BN as a function of temperature and pressure. (a) compares our theoretical Raman frequency with the fitted form in Eqs. (9) and (10). (b) compares our calibration at 300 K with experimental results from [25,26] extrapolated to higher pressures. The black circles are the QMC frequencies (errors are smaller than the symbols), while the blue solid line gives the fit. The lower inset gives an expanded view at low pressure, in which the shaded region gives the statistical confidence region. The upper inset gives the variation with temperature.

We have presented a fully *ab initio* pressure calibration based on quantum Monte Carlo simulations, and have introduced a method for all-electron simulations of solids to eliminate bias from pseudopotentials. This method should be applicable to at least first-row solids, allowing increased accuracy in the study of other materials and providing a new benchmark for other methods. The only remaining systematic error in the static contribution to the EOS is from the fixed-node approximation used in DMC. For simple materials such as $c$-BN this error should be quite small, and tends to cancel between different volumes. Thus we believe the EOS is robust enough to be used directly in experiment as a primary pressure calibrant, and can be used to cross calibrate scales based on other materials. Since the accuracy should not depend on compression, our calibration can be used up to 900 GPa.

This work was supported under the National Science Foundation Grant EAR-0530282. This research used resources of the National Center for Computational Sciences and the Center for Nanophase Materials Sciences, which are sponsored by the U.S. Department of Energy. This research was supported in part by the National Science Foundation through TeraGrid resources provided by the NCSA and NICS under TG-MCA07S016, TG-MCA93S030, and TG-EAR080015. We thank A. Goncharov, F. Mauri, and M. Lazzeri for helpful suggestions and discussions.

*esler@uiuc.edu

[1] Yingwei Fei *et al.*, Proc. Natl. Acad. Sci. U.S.A. **104**, 9182 (2007).
[2] H. K. Mao, J. Xu, and P. M. Bell, J. Geophys. Res. **91**, 4673 (1986).
[3] Chang-Sheng Zha, Ho-kwang Mao, and Russell J. Hemley, Proc. Natl. Acad. Sci. U.S.A. **97**, 13 494 (2000).
[4] J. R. Asay *et al.*, Int. J. Impact Eng. **23**, 27 (1999).
[5] J. Remo and M. Furnish, Int. J. Impact Eng. **35**, 1516 (2008).
[6] W. B. Holzapfel, High Press. Res. **25**, 87 (2005).
[7] A. F. Goncharov *et al.*, Phys. Rev. B **75**, 224114 (2007).
[8] W. M. C. Foulkes, L. Mitas, R. J. Needs, and G. Rajagopal, Rev. Mod. Phys. **73**, 33 (2001).
[9] Ryo Maezono, A. Ma, M. D. Towler, and R. J. Needs, Phys. Rev. Lett. **98**, 025701 (2007).
[10] J. Kolorenč and L. Mitas, Phys. Rev. Lett. **101**, 185502 (2008).
[11] R. J. Needs, M. D. Towler, N. D. Drummond, and P. L. Rios, J. Phys. Condens. Matter **22**, 023201 (2010).
[12] Jeongnim Kim *et al.*, QMCPACK simulation suite http://qmcpack.cmscc.org.
[13] J. K. Dewhurst *et al.*, The EXCITING FP-LAPW code, http://exciting.sourceforge.net.
[14] A. J. Williamson *et al.*, Phys. Rev. B **55**, R4851 (1997).
[15] S. Chiesa, D. M. Ceperley, R. M. Martin, and M. Holzmann, Phys. Rev. Lett. **97**, 076404 (2006).
[16] J. R. Trail and R. J. Needs, J. Chem. Phys. **122**, 174109 (2005); **122**, 014112 (2005).
[17] M. Burkatzki, C. Filippi, and M. Dolg, J. Chem. Phys. **126**, 234105 (2007).
[18] Zhigang Wu and R. E. Cohen, Phys. Rev. B **73**, 235116 (2006).
[19] Opium pseudopotentials, http://opium.sourceforge.net.
[20] See supplementary material at http://link.aps.org/supplemental/10.1103/PhysRevLett.104.185702.
[21] S. Baroni *et al.*, J. Phys. Condens. Matter **21**, 395502 (2009).
[22] J. Furthmüller, J. Hafner, and G. Kresse, Phys. Rev. B **50**, 15 606 (1994).
[23] P. Vinet *et al.*, J. Phys. Condens. Matter **1**, 1941 (1989).
[24] F. Datchi, A. Dewaele, Y. Le Godec, and P. Loubeyre, Phys. Rev. B **75**, 214104 (2007).
[25] F. Datchi and B. Canny, Phys. Rev. B **69**, 144106 (2004).
[26] A. F. Goncharov, J. C. Crowhurst, J. K. Dewhurst, and S. Sharma, Phys. Rev. B **72**, 100104(R) (2005).
[27] I. V. Alexandrov *et al.*, *High Pressure Study of Diamond, Graphite and Related Materials* (Terrepub AGU, Washington-Tokyo, 1992), p. 409.